Article

Enhancing the Linearity and Stability of a Fabric-Based Strain Sensor with Microfolded Graphene Structures

Rongqing Xu [1], Xin Zheng [2], Miao Chen [3], Lijun Sun [1], Jiangwei Chen [1], Fangfang Wang [4],* and Yun Ma [5]

[1] College of Electronic and Optical Engineering & College of Microelectronics, Nanjing University of Posts and Telecommunications, Nanjing 210049, China; xurq@njupt.edu.cn (R.X.); slj8006@163.com (L.S.); jwchen69@njupt.edu.cn (J.C.)

[2] College of Automation & College of Artificial Intelligence, Nanjing University of Posts and Telecommunications, Nanjing 210049, China

[3] Office of Scientific R&D, Nanjing University of Posts and Telecommunications, Nanjing 210049, China; kjbmb@njupt.edu.cn

[4] School of Art and Design, Yangzhou University, Yangzhou 225009, China

[5] Jiangsu College of Engineering and Technology, Nantong 226007, China; ntmayun@126.com

* Correspondence: wffsjj@ntu.edu.cn; Tel.: +86-025-85866504

check for updates

Abstract: Fabric-based strain sensors can be seamlessly integrated into wearable systems for monitoring various physiological signals. Although many different approaches have been proposed to increase the sensitivity of the fabric-based strain sensor, the linearity and stability in large strains are still challenging. In this paper, a fabric-based strain sensor with good linearity and stability was fabricated via a three-step dip-coating method. Specifically, the combination of multiwall carbon nanotubes and reduced graphene oxide was used as the conductive material to enhance the stability. Meanwhile, microfolded structures between two reduced graphene oxide layers were created via pre-stretching to achieve good linearity. Through mechanical experiments, the performance of the fabric-based strain sensor was characterized. In addition, the practical applications of the strain sensor were demonstrated by monitoring different physiological signals.

---

1. Introduction

Soft strain sensors capable of withstanding large strains are found as important elements in various applications, such as wearable devices for monitoring human activity [1], and soft robotics for detecting deformation states [2]. With the developments in materials and fabrication technologies, different measurement mechanisms such as capacitance [3,4], resistivity [5], piezoelectricity [6], and inductance [7] have been successfully applied to develop soft strain sensors. Especially, soft resistive strain sensors based on the strain-resistance response have attracted extensive interest due to their advantages in easy fabrication, low power consumption, and simple readout circuit [8].

Generally, a soft resistive sensor is a two-part composite, i.e., a conductive film as the sensing part and an elastic substrate as the supporting part. After adhering the two parts together, they share the same deformation pattern. Therefore, the stretch of the substrate changes the conductive paths in the conductive film, leading to the resistance variation. Apparently, the materials utilized in the two parts have great impacts on the performances of the soft strain sensors. To date, the preferential

conductive materials for fabricating the conductive films are nanomaterials due to superior electrical, mechanical, and thermal properties. As a typical nanomaterial, the applications of graphene and its derivatives, including graphene oxide (GO) and reduced graphene oxide (rGO), in soft strain sensors, have been deeply discussed in the literature [9–11]. As the unique hexagonal lattice formed by its internal carbon atoms, graphene shows excellent optical, thermal, mechanical, and electrical properties [12]. For example, the resistivity of graphene is only about 10–8 Ω/m, which is much lower than that of pure copper (0.017 Ω/m) [13]. Additionally, the cross-sectional thermal conductivity of bulk GO is 100 times lower than that of graphite [14]. At present, the preparation methods of graphene mainly include mechanical exfoliation, graphite oxide reduction, chemical vapor deposition, and silicon carbide epitaxial growth [15]. Among them, the graphite oxide reduction method is not only low in cost, but also can realize the mass-production of graphene. With the development of the fabrication technology, graphene-based materials have experienced in-depth developments in many advanced fields. For example, in the light modulation field, graphene-based metasurfaces—due to the high absorption rate of electromagnetic waves of many different frequencies—have attracted wide interest [16–18]. In the field of flexible electronic devices, the graphene-based touch screens and electronic papers have excellent bending capability and stretchability [19].

Although graphene has many outstanding merits, such as cost-effectiveness, biocompatibility, and surface area (ultrahigh), its fragility restricts the stretch of a planar graphene film in a narrow range. In order to overcome this restriction, the textured graphene films with different microstructures/patterns (e.g., buckling pattern [20], kirigami-structured pattern [21], porous network structure [22]) have been proposed. For a strain sensor, it was found that the textured graphene films not only broaden its measurement range, but also improve its linearity, and even add new functionalities such as the detection of organic gas [23]. About the materials of the elastic substrates, elastomers with high stretchability and good elasticity such as polydimethylsiloxane (PDMS), Ecoflex, and thermoplastic elastomers (TPEs) are commonly adopted. The influence of the elastic substrate on the strain sensor was reviewed in [8]. Recently, fabric-based strain sensors using fabrics as the elastic substrates have also received widespread attention, which show advantages in diverse structures and strong adhesion of conductive nanomaterials over the elastomer-based strain sensors [24]. Furthermore, the fabric-based strain sensors can provide better wearing comfort, thereby being more suitable for wearable sensing devices.

At present, one of the most popular techniques for applying graphene to fabricate the fabric-based strain sensor is coating, including dip-coating, spray coating, and roller coating [25]. For example, based on dip-coated conductive graphene networks, fabric-based strain sensors were manufactured by using nylon/spandex knitted fabric [26], non-woven fabric [27], nylon/polyurethane fabric [28], and polyester knitted elastic bands [29]. In addition, multi-functional fabric sensors were fabricated by coating conductive networks of graphene, which are capable of measuring strain, pressure, and vibrations, and blocking ultraviolet (UV) [30,31]. Although the high sensitivity and stretchability of the fabric-based sensors fabricated by coating have been achieved in the literature mentioned above, high linearity and stability are still challenging. For example, it is found that the resistance of a polyurethane (PU) fiber coated by Ag nanowires (AgNWs) at the zero strain experienced a substantial drift after cycling deformations, increasing 0.37 times with respect to its initial value after 50 cycles [32]. In principle, one of the main reasons arising the drift is the poor stability of the conductive network, especially the irreversible deconstruction of some conductive paths. As an approach to increase the stability, the combination of conductive filler materials of different dimensions was used [33]. For example, the stability of a PDMS-based strain sensor was much improved by hybridizing carbon nanofibers (CNFs) with graphene nanoplates (GNPs) [34].

In this study, with the expectation of enhancing the linearity and stability of the fabric-based strain sensor, we dip-coated the fabric with three conductive networks, i.e., one multi-wall carbo nanotubes (MWCNTs) network and two rGO networks. In particular, microfolded structures between the rGO networks were developed by stretching the fabric during dip-coating process. In addition,

we also improved the durability of the strain sensor by strengthening the interactions between the conductive nanomaterials and the fabric surfaces via covalent immobilization [35]. The rest of the paper is organized as follows. Section 2 presents the materials and fabrication process, which is followed by sensor characterization and mechanical experiments in Section 3. Then, Section 4 gives some potential applications of the strain sensor in human physiological signals monitoring. Finally, the conclusions are drawn in Section 5.

2. Materials and Sensor Fabrication

2.1. Materials

Considering its good stretchability and elasticity, a nylon spandex fabric, consisting of 17% polyurethane (PU) fiber and 83% polyamide (PA) fiber, was bought on the market. Hydrazine hydrate solution (50%) and absolute ethanol were purchased from Sinopharm Chemical Reagent Co., Ltd. Graphene oxide (XF002-1, diameter: 0.5–5 µm, thickness: 0.8–1.2 nm, purity: about 99%) and MWCNTs powder (XFM01, outer diameter: 5–15 nm, length: 10–30 µm, purity: >95%, specific surface area (SA): >200 m^2/g, true density: 2.1 g/cm^3, electric conductivity (EC): >100 s/cm) were obtained from Nanjing XFNANO Materials Co., Ltd.

### 2.2. Fabrication of Fabric-Based Strain Sensor

Although the rGO-coated fabric can be produced by coating GO followed by reduction, the toxicity of most reducing agent lowers the wearing safety of the obtained fabric. Therefore, we directly coated the fabric with rGO. To avoid the agglomeration in high-concentration rGO dispersion, *N,N′*-(cyclohexa-2,5-diene-1,4-diylidene) bis (2-hydroxy-*N*-(2-hydroxy-3-(4-(trihydroxysilyl)butoxy) propyl)-3-(4-(trihydroxysilyl)butoxy)propan-1 -ami-nium) (TSiPD) dispersant synthesized according to the procedures in [35,36] was used. Meanwhile, since ample amounts of silanol groups were introduced by TSiPD, the dehydration condensation between the silanol groups and hydroxyl groups of the cotton fibers made rGO strongly adhere to the fiber surfaces.

A 5 mg/mL graphene oxide solution was prepared by adding graphene oxide into deionized water. After homogeneously dispersing GO under a 40 kHz ultrasound environment, hydrazine hydrate solution was added to the graphene oxide solution via a dropper. Then, the mixed solution was placed in a water bath and heated at 90 °C for 2 h for hydrothermal reduction. Finally, mixing the GO solution and the TSiPD solution followed by sonication produced a homogeneous mixture of TSiPD and rGO. Similarly, the mixture of TSiPD and MWCNTs dispersion was obtained by adding MWCNTs into the TSiPD solution, sonicating for 10 min, and standing for 1 h.

After pretreating the nylon spandex fabric by alternate sonications in ethanol and deionized water, the conductive fabric was fabricated through three dip-coating steps which are schematically shown in Figure 1. During the first dip-coating, the nylon spandex fabric was immersed in the MWCNTs-TSiPD mixture under ultrasonic environment. After 10 min immersion, the fabric coated with MWCNTs networks was taken out and dried in a 70 °C blast oven for 30 min. For the second dip-coating, immersing the fabric in the rGO-TSiPD mixture was performed in the same manner as the first dip-coating. In order to create microfolded rGOs structures, we stretched the obtained rGO/MWCNTs fabric up to the strain of 50%, and fixed two ends of the stretched fabric on a glassware with transparent tape. Successively, the second rGO film was generated by immersing the stretched fabric in the RGO-TSiPD mixture again. Finally, the conductive fabric was obtained by releasing it to its original state. Based on the obtained conductive fabric, a MWCNTs/rGO/rGO strain sensor can be obtained by coating conductive silver paste, leading out the wires.

In general, the greater the pre-stretch, the more micro-folded rGO structures in the conductive fabric. However, when the stretching range is too large, the violent deformation, resulting to a long recovery time during releasing the fabric, reduces the dynamic response of the sensor. Through many

trial experiments, it was found that the strain sensor obtained with the pre-tensile strain of 50% achieves a good compromise between the dynamic and the static performances.
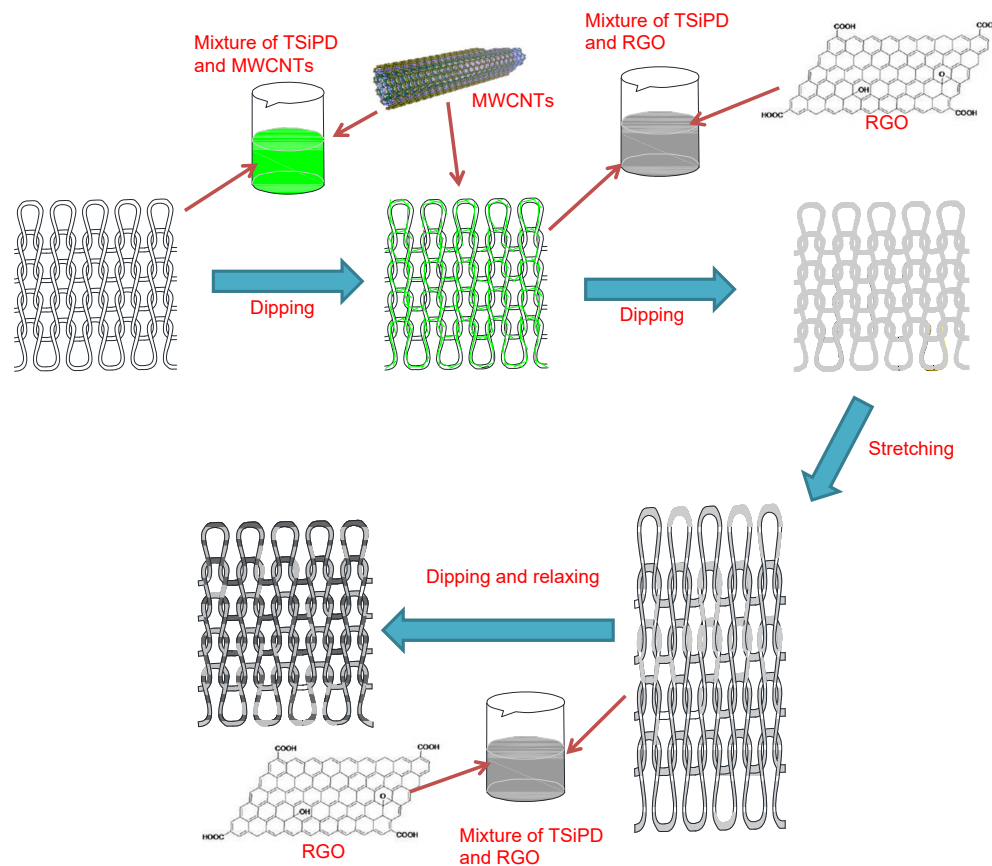
Figure 1. A schematic illustration about fabricating conductive fabric through three dip-coating steps.

3. Results

3.1. Characterization

The surface morphology of the conductive fabric was characterized by a scanning electron microscope (SEM) shown in Figure 2. It can be seen that the rGOs homogeneously coated the fabric threads. In order to show the microfolded rGO structures, a rectangle area of the coated fabric in Figure 2a is zoomed in on. As shown in Figure 2b, two microfolded rGO layers on a single fabric thread generated by two rGO dip-coatings can be clearly distinguished. When stretching the conductive fabric, relative sliding between the lower rGO layer and the upper rGO layer causes their overlapping area to decrease, thereby leading to the increase in the contact resistance between them.

3.2. Properties of the Strain Sensor

We first studied the sensitivity and linearity of the strain sensor; the resistance was measured by a digital source meter. After fixing two ends of the sensor to two tensile grips of an universal machine, the sensor was quasi-statically stretched to a maximum strain of 21% with a 3% increment per step. The measured data relating the relative change in resistance to strain is shown in Figure 3, where ΔR and R_0 are the resistance change and the initial resistance, respectively. In order to demonstrate the effect played by the microfolded rGO structures, the response of a MWCNTs/rGO sensor which was fabricated without the third dip-coating step is also presented. It can be seen that although the sensitivity of the MWCNTs/rGO sensor is better at small strains, the sensitivity of the MWCNTs/rGO/rGO sensor stays good over entire strains. This can be explained by the sensing

mechanism in Figure 4 where the cyan rectangle and the pink curve respectively represent the rGO and MWCNTs. When the sensor is stretched, the decrease of the overlapping area of the upper and lower rGO sheets due to their relative sliding causes the contact resistance to increase. It is worth noting that the contact resistance is the horizontal-direction resistance between two rGO sheets, which is schematically shown in Figure 4. Compared with the breakdown of the conductive paths of rGO sheets, the change of the conductive path caused by the slip of the overlapping area was not dramatic, thereby lowering the sensitivity at small strains. On the other hand, since the contact resistance between two rGO layers is linearly proportional to the strain [37], the obtained sensor has good linearity.
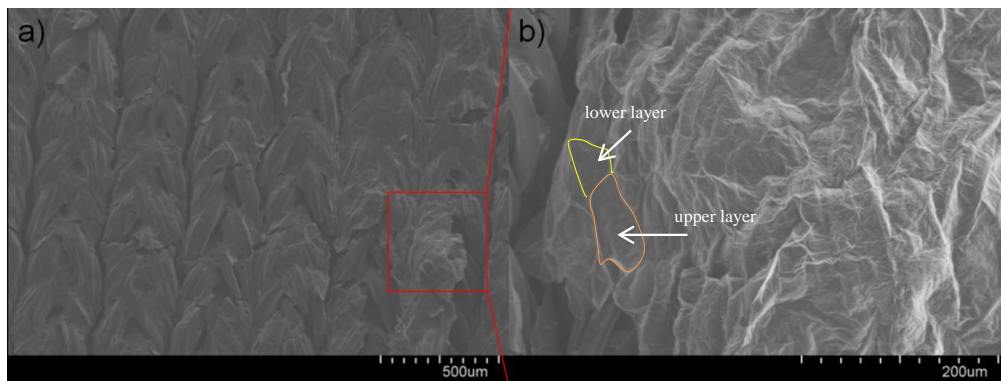

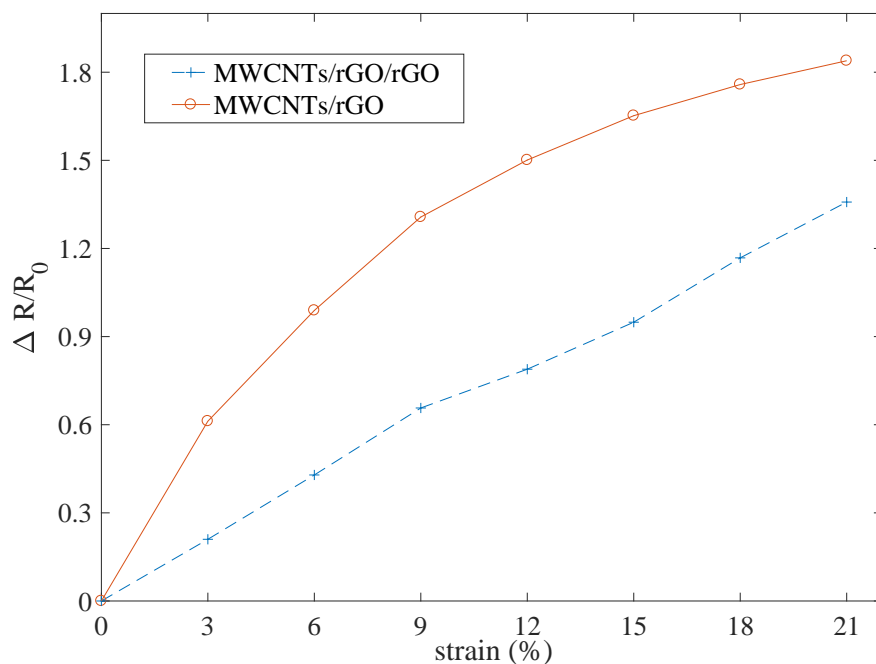**Figure 2.** SEM characterization of the conductive fabric.

Figure 3. Linearity of the fabric-based strain sensors with and without microfolded rGO structures.

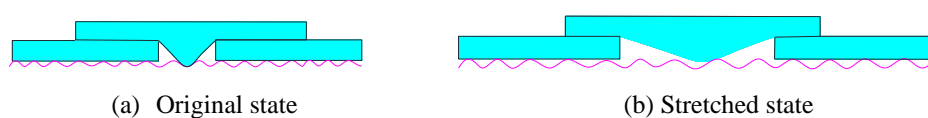(a) Original state   (b) Stretched state

Figure 4. Schematics of the mechanism due to MWCNTs and two rGO conductive networks.

As mentioned above, another aspect attracting our attention was the stability of the strain sensor. It is well known that the irreversible breakage of the conductive paths is the main reason for the poor stability. Due to the large aspect ratio of MWCNTs, it was expected to achieve good

stability in combination with rGO. Ten stretching-releasing cycles were exerted on the fabric-based MWCNTs/rGO/rGO strain sensor, and the measured relative change in resistance is presented in Figure 5. For comparison, the corresponding response of a rGO/rGO strain sensor without the first dip-coating step is also shown. It can be seen that the stability of the MWCNTs/rGO/rGO strain sensor was better compared to the rGO/rGO strain sensor in two aspects, i.e., the overall relative change in resistance between each cycle, and the recovery of its value at the zero strain.
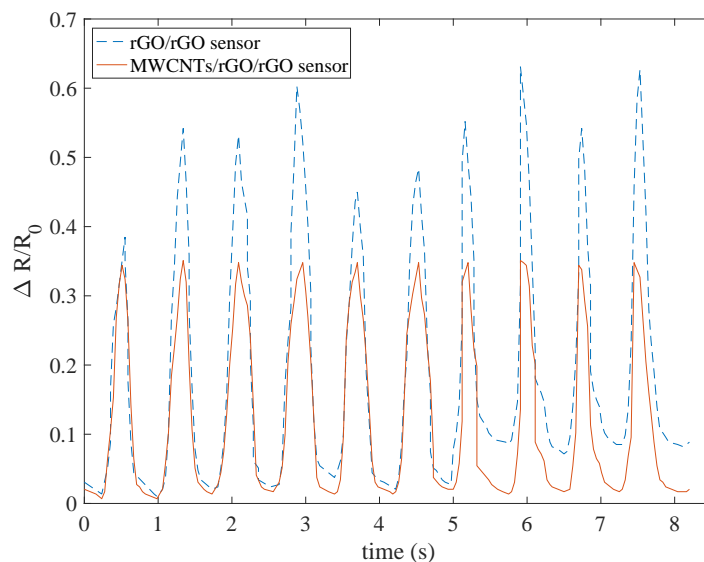
Figure 5. Stability of the fabric-based strain sensors with and without MWCNTs.

Furthermore, the effect of rGO concentration on the sensor sensitivity was also studied. Besides the strain sensor coated by 5 mg/mL rGO solution, another one was developed by using 10 mg/mL rGO solution. The two sensors experienced the same stretch; the measured data are shown in Figure 6. It can be seen that, irrespective of the rGO concentration, both the two sensors have good linearities over the strain range 0~21%. However, the higher the rGO concentration, the higher the sensitivity of the sensor. The reason is that more rGO sheets can be deposited on the fabric surface when using the higher rGO concentration; thus, more microfolded structures are formed.
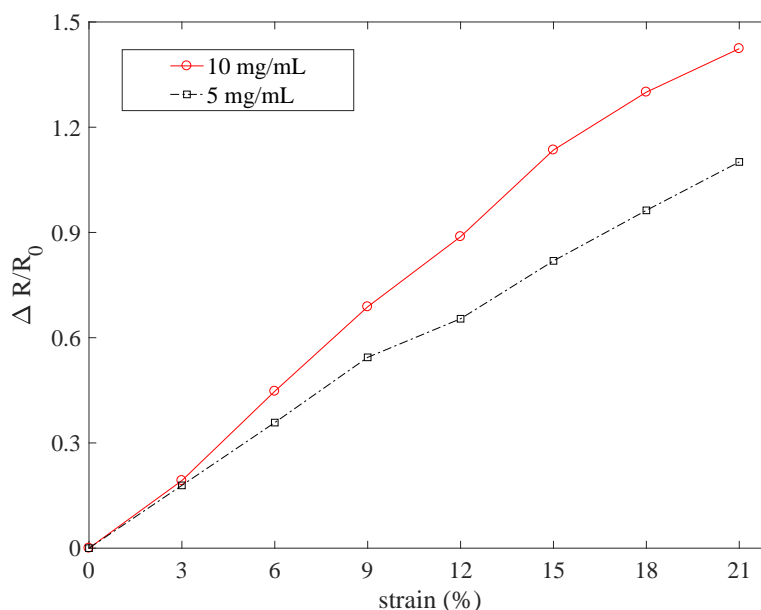
**Figure 6.** The effect of rGO concentration on the sensor's response.

4. Applications

Soft strain sensors can be applied to wearable personal health monitoring devices to assist in injury prevention or disease diagnosis. Compared to membrane-based strain sensors, the fabric-based strain sensors are more convenient in monitoring human health.

4.1. Finger Bending Detection

The fabric-based strain sensor was first applied to monitor finger flexion experiencing large deformations. After attaching the sensor to the proximal interphalangeal (PIP) joint of the index finger at its straight state, the relative changes in resistance for three consecutive finger bendings $(0\text{–}45°, 0\text{–}90°, \text{and } 0\text{–}135°)$ were measured as shown in Figure 7a. It can be seen the relative change in resistance increases as the finger bending increases. The larger the finger bending, the greater the relative change in resistance. Furthermore, when the finger returns to be straight, the relative change in resistance recovers to be about zero.
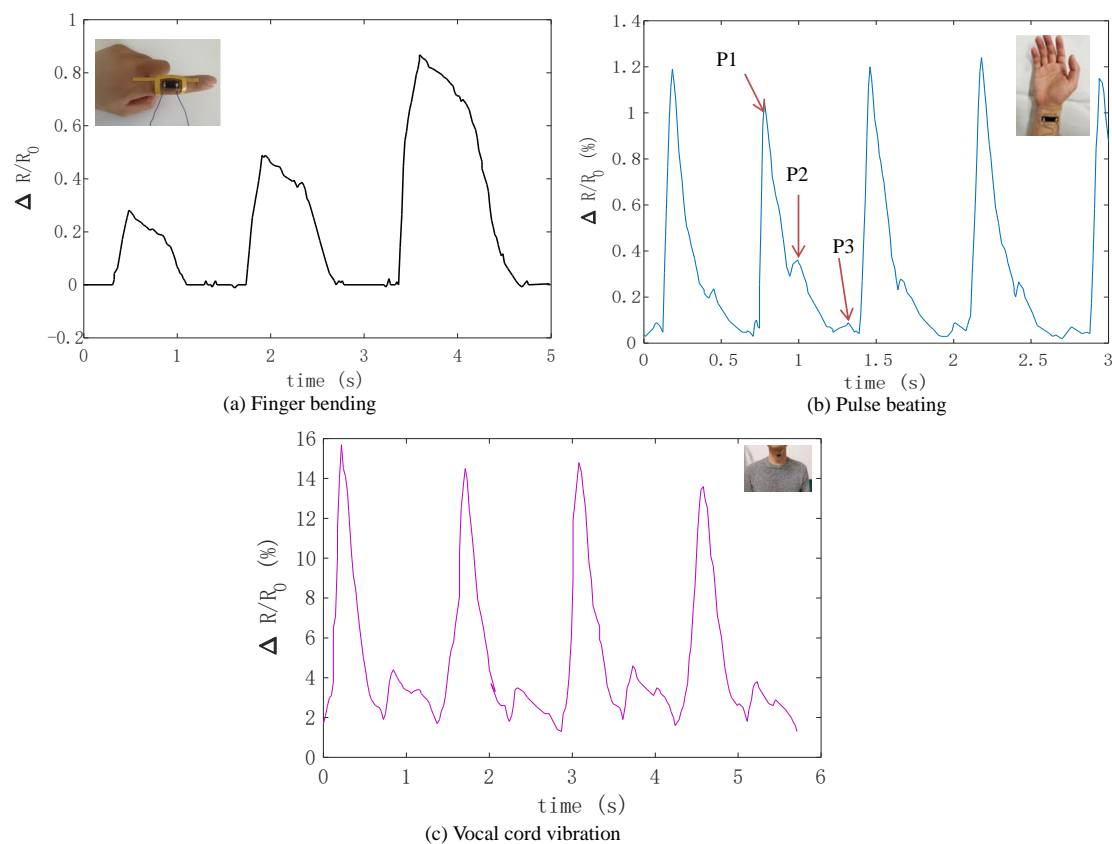
Figure 7. Applications of the fabric-based MWCNTs/rGO/rGO strain sensor in physiological signal detection.

4.2. Human Pulse Monitoring

Human pulse was monitored to test the ability of the strain sensor to measure small strains. The radial artery sitting on the thumb side of the wrist is commonly used to clinically measure heart rate in traditional Chinese medicine. Therefore, to mimic the actual application, we attached the strain sensor to the radial artery of the wrist via transparent tape. The wave-form signal of the strain sensor in 3 s is shown in Figure 7b. As can be seen, although the relative change in resistance is very small with its maximum at 1.2%, good measurement stability can still be achieved. Clearly, there are four stable pulse-beating cycles with each, including three local peak values, P1, P2, and P3, which respectively represent pulse beating, left ventricular systolic pressure, and lower body reflection. Based on these

peak values, certain diseases can be diagnosed. For example, the ratio of P2 and P1 can be used as an evaluation criterion for the degree of arteriosclerosis which is a common disease of the elderly.

4.3. Measurement of Vocal Cord Vibration

In order to expand the application of the fabric-based strain sensor, the vocal cord vibrations during speaking were measured—this is important for developing artificial throats [38]. Normal voice production relies on three organs, i.e., the lung, larynx, and sound teeth. When producing sound, the vocal folds close from the open state. As air expelled by the lung passes through the closed vocal folds, they vibrate. Meanwhile, the tension length of the vocal folds alters with changes in pitch. Finally, sound produced by the vibrations of the vocal folds is modified via sound teeth. In general, the main vocal organ is the larynx located in the throat. Therefore, the strain sensor was attached to the throat for measuring the vocal cord vibrations, as shown in the inset of Figure 7c.

During the measurement, the speaker was requested to repeatedly vocalize two Chinese characters, "Nan" and "Jing", while keeping the speech rate as smooth as possible. Figure 7c shows the signals of the relative change in resistance for four repeated pronunciations. There are two local peak values for saying "Nan Jing" each time. The first local peak is higher, which may be due to the greater vibration caused by the Chinese character "Nan". When the Chinese character "Jing" is said, the vocal cords contract and the throat node vibrations are small, resulting in the second local peak.

4.4. Potential Industrial Applications

Besides motion monitoring and disease diagnosis, the strain sensor can also be used in a broad range of fields, including automotive, power systems, and robotics, while aiming to create applications in solution services targeting the Internet of Things. For example, amount of strain sensors employed in automotive devices and robots can accurately measure strain changes caused by forces exerted on those devices [39,40]. In this way, it will be possible to efficiently manage and control status of those, to enable the smooth operation of devices, and to diagnose the signs of potential failures. Compared with other exist strain sensors, our fabric-based strain sensor possesses the following two advantages. First, the softness of the fabric strain sensor makes it conveniently conform to the curvilinear surfaces of complex devices. Second, the fabric-based strain sensor due to TSiPD bonding has much better durability.

5. Conclusions

To improve the linearity and stability of the fabric-based strain sensor, this paper proposes a three-step dip-coating method by using MWCNTs and rGOs. By means of coating the stretched fabric, the micro-folded structures consisting of two rGO layers are formed. Therefore, the sensing mechanism is dependent on the variation of the contact resistance between two rGO layers, which has a linear relation with the strain of the fabric. The SEM characterization and experiments validated that the fabric-based MWCNTs/rGO/rGO sensor possesses good linearity and stability. Additionally, the potential applications of the fabric-based strain sensor were demonstrated by the stable and reliable measurements of different physiological signals. In future, the Wheatstone bridge circuit instead of digital source meter will be implemented to measure the strain signals. This could not only further improve the sensor's accuracy but also enhance its portability. Moreover, in order to widen the measurement frequency of the sensor, we will investigate the sensor's performance by adopting a metasurface fabric as the substrate.

Author Contributions: Conceptualization, F.W. and R.X.; methodology, R.X.; software, L.S.; validation, X.Z.; formal analysis, M.C.; resources, Y.M.; data curation, L.S.; writing—original draft preparation, R.X.; writing—review and editing, X.Z.; visualization, J.C.; supervision, F.W.; project administration, F.W.; funding acquisition, F.W. All authors have read and agreed to the published version of the manuscript.

Conflicts of Interest: The authors declare no conflict of interest. The funders had no role in the design of the study; in the collection, analyses, or interpretation of data; in the writing of the manuscript, or in the decision to publish the results.

References

1. Hughes, J.; Iida, F. Multi-functional soft strain sensors for wearable physiological monitoring. *Sensors* **2018**, *18*, 3822. [CrossRef]

2. Park, M.; Ohm, Y.; Kim, D.; Park, Y. Multi-material soft strain sensors with high gauge factors for proprioceptive sensing of soft bending actuators. In Proceedings of the 2019 2nd IEEE International Conference on Soft Robotics (RoboSoft), Seoul, Korea , 14–18 April 2019; pp. 384–390.

3. Frutiger, A.; Muth, J.T.; Vogt, D.M.; Menguc, Y.; Campo, A.B.; Valentine, A.D.; Walsh, C.J.; Lewis, J.A. Capacitive soft strain sensors via multicore–shell fiber printing. *Adv. Mater.* **2015**, *27*, 2440–2446. [CrossRef]

4. Shintake, J.; Nagai, T.; Ogishima, K. Sensitivity improvement of highly stretchable capacitive strain sensors by hierarchical auxetic structures. *Front. Robot. AI* **2019**, *6*, 127. [CrossRef]

5. Jiang, D.; Wang, Y.; Li, B.; Sun, C.J.; Wu, Z.; Yan, H.; Xing, L.; Qi, S.; Li, Y.; Liu, H.; et al. Flexible sandwich structural strain sensor based on silver nanowires decorated with self-healing substrate. *Macromol. Mater. Eng.* **2019**, *304*, 1900074. [CrossRef]

6. Ahn, S.; Cho, Y.; Park, S.; Kim, J.; Sun, J.; Ahn, D.; Lee, M.; Kim, D.; Kim, T.; Shin, H.; et al. Wearable multimode sensors with amplified piezoelectricity due to the multi local strain using 3D textile structure for detecting human body signals. *Nano Energy* **2020**, *74*, 104932. [CrossRef]

7. Tavassolian, M.; Cuthbert, T.J.; Napier, C.; Peng, J.; Menon, C. Textile-based inductive soft strain sensors for fast frequency movement and their application in wearable devices measuring multiaxial hip joint angles during running. *Adv. Intell. Syst.* **2020**, *2*, 1900165. [CrossRef]

8. Amjadi, M.; Kyung, K.; Park, I.; Sitti, M. Stretchable, skin-mountable, and wearable strain sensors and their potential applications: A review. *Adv. Funct. Mater.* **2016**, *26*, 1678–1698. [CrossRef]

9. Mehmood, A.; Mubarak, N.; Khalid, M.; Walvekar, R.; Abdullah, E.; Siddiqui, M.; Baloch, H.A.; Nizamuddin, S.; Mazari, S. Graphene based nanomaterials for strain sensor application—A review. *J. Environ. Chem. Eng.* **2020**, *8*, 103743. [CrossRef]

10. Huang, H.; Su, S.; Wu, N.; Wan, H.; Wan, S.; Bi, H.; Sun, L. Graphene-based sensors for human health monitoring. *Front. Chem.* **2019**, *7*, 399. [CrossRef]

11. Yee, M.J.; Mubarak, N.; Abdullah, E.; Khalid, M.; Walvekar, R.; Karri, R.R.; Nizamuddin, S.; Numan, A. Carbon nanomaterials based films for strain sensing application—A review. *Nano-Struct. Nano-Objects* **2019**, *18*, 100312. [CrossRef]

12. Kinloch, I.A.; Suhr, J.; Lou, J.; Young, R.J.; Ajayan, P.M. Composites with carbon nanotubes and graphene: An outlook. *Science* **2018**, *362*, 547–553. [CrossRef] [PubMed]

13. Yang, Y.; Ping, Y.; Gong, Y.; Wang, Z.; Fu, Q.; Pan, C. Ag/graphene composite based on high-quality graphene with high electrical and mechanical properties. *Prog. Nat. Sci. Mater. Int.* **2019**, *29*, 384–389. [CrossRef]

14. Meng, Q.L.; Liu, H.; Huang, Z.; Kong, S.; Jiang, P.; Bao, X. Tailoring thermal conductivity of bulk graphene oxide by tuning the oxidation degree. *Chin. Chem. Lett.* **2017**, *29*, 711–715. [CrossRef]

15. Yin, P.T.; Shah, S.; Chhowalla, M.; Lee, K.B. Design, Synthesis, and Characterization of Graphene–Nanoparticle Hybrid Materials for Bioapplications. *Chem. Rev.* **2015**, *115*, 2483–2531. [CrossRef]

16. Barzegar-Parizi, S. Realization of wide-angle and wideband absorber using metallic and graphene-based metasurface for mid-infrared and low THz frequency. *Opt. Quantum Electron.* **2018**, *50*, 378. [CrossRef]

17. Spada, L.L.; Spooner, C.; Haq, S.; Hao, Y. Curvilinear metasurfaces for surface wave manipulation. *Sci. Rep.* **2019**, *9*, 3107. [CrossRef]

18. Spada, L.L.; Vegni, L. Metamaterial-based wideband electromagnetic wave absorber. *Opt. Express* **2016**, *24*, 5763–5772. [CrossRef]

19. Novoselov, K.S.; Falko, V.; Colombo, L.; Gellert, P.R.; Schwab, M.G.; Kim, K. A roadmap for graphene. *Nature* **2012**, *490*, 192–200. [CrossRef]

20. Song, J.; Tan, Y.; Chu, Z.; Xiao, M.; Li, G.; Jiang, Z.; Wang, J.; Hu, T. Hierarchical reduced graphene oxide ridges for stretchable, wearable, and washable strain sensors. *ACS Appl. Mater. Interfaces* **2019**, *11*, 1283–1293. [CrossRef]

21. Xu, K.; Lu, Y.; Honda, S.; Arie, T.; Akita, S.; Takei, K. Highly stable kirigami-structured stretchable strain sensors for perdurable wearable electronics. *J. Mater. Chem. C* **2019**, *7*, 9609–9617. [CrossRef]

22. Pang, Y.; Tian, H.; Tao, L.; Li, Y.; Wang, X.; Deng, N.; Yang, Y.; Ren, T.L. Flexible, highly sensitive, and wearable pressure and strain sensors with graphene porous network structure. *ACS Appl. Mater. Interfaces* **2016**, *8*, 26458–26462. [CrossRef] [PubMed]

23. Jia, Y.; Yue, X.; Wang, Y.; Yan, C.; Zheng, G.; Dai, K.; Liu, C.; Shen, C. Multifunctional stretchable strain sensor based on polydopamine/reduced graphene oxide/electrospun thermoplastic polyurethane fibrous mats for human motion detection and environment monitoring. *Compos. Part B Eng.* **2020**, *183*, 107696. [CrossRef]

24. Seyedin, S.; Zhang, P.; Naebe, M.; Qin, S.; Chen, J.; Wang, X.; Razal, J.M. Textile strain sensors: A review of the fabrication technologies, performance evaluation and applications. *Mater. Horiz.* **2019**, *6*, 219–249. [CrossRef]

25. Liu, W.; Huang, Y.; Peng, Y.; Walczak, M.; Wang, D.; Chen, Q.; Liu, Z.; Li, L. Stable wearable strain sensors on textiles by direct laser writing of graphene. *ACS Appl. Nano Mater.* **2020**, *3*, 283–293. [CrossRef]

26. Lee, H.; Glasper, M.J.; Li, X.; Nychka, J.A.; Batcheller, J.; Chung, H.; Chen, Y. Preparation of fabric strain sensor based on graphene for human motion monitoring. *J. Mater. Sci.* **2018**, *53*, 9026–9033. [CrossRef]

27. Du, D.; Li, P.; Ouyang, J. Graphene coated nonwoven fabrics as wearable sensors. *J. Mater. Chem. C* **2016**, *4*, 3224–3230. [CrossRef]

28. Cai, G.; Yang, M.; Xu, Z.; Liu, J.; Tang, B.; Wang, X. Flexible and wearable strain sensing fabrics. *Chem. Eng. J.* **2017**, *325*, 396–403. [CrossRef]

29. Reddy, K.R.; Gandla, S.; Gupta, D. Highly sensitive, rugged, and wearable fabric strain sensor based on graphene clad polyester knitted elastic band for human motion monitoring. *Adv. Mater. Interfaces* **2019**, *6*, 1900409. [CrossRef]

30. Yuan, W.; Yang, J.; Yang, K.; Peng, H.; Yin, F. High-performance and multifunctional skinlike strain sensors based on graphene/springlike mesh network. *ACS Appl. Mater. Interfaces* **2018**, *10*, 19906–19913. [CrossRef]

31. Wang, S.; Ning, H.; Hu, N.; Liu, Y.; Liu, F.; Zou, R.; Huang, K.; Wu, X.; Weng, S.; Alamusi. Environmentally-friendly Additionally, Multifunctional Graphene-silk Fabric Strain Sensor For Human-motion Detection. *Adv. Mater. Interfaces* **2020**, *7*, 1901507. [CrossRef]

32. Lu, Y.; Jiang, J.; Yoon, S.; Kim, K.S.; Kim, J.H.; Park, S.; Kim, S.H.; Piao, L. High-performance stretchable conductive composite fibers from surface-modified silver nanowires and thermoplastic polyurethane by wet spinning. *ACS Appl. Mater. Interfaces* **2018**, *10*, 2093–2104. [CrossRef]

33. Zhang, F.; Wu, S.; Peng, S.; Sha, Z.; Wang, C.H. Synergism of binary carbon nanofibres and graphene nanoplates in improving sensitivity and stability of stretchable strain sensors. *Compos. Sci. Technol.* **2019**, *172*, 7–16. [CrossRef]

34. Shi, J.; Li, X.; Cheng, H.; Liu, Z.; Zhao, L.; Yang, T.; Dai, Z.; Cheng, Z.; Shi, E.; Yang, L.; et al. Graphene reinforced carbon nanotube networks for wearable strain sensors. *Adv. Funct. Mater.* **2016**, *26*, 2078–2084. [CrossRef]

35. Cui, J.; Zhou, S. Highly conductive and ultra-durable electronic textiles via covalent immobilization of carbon nanomaterials on cotton fabric. *J. Mater. Chem. C* **2018**, *6*, 12273–12282. [CrossRef]

36. Cui, J.; Zhou, S. High-concentration self-cross-linkable graphene dispersion. *Chem. Mater.* **2018**, *30*, 4935–4942. [CrossRef]

37. Liu, Q.; Chen, J.; Li, Y.; Shi, G. High-performance strain sensors with fish-scale-like graphene-sensing layers for full-range detection of human motions. *ACS Nano* **2016**, *10*, 7901–7906. [CrossRef] [PubMed]

38. Wei, Y.; Qiao, Y.; Jiang, G.; Wang, Y.; Wang, F.; Li, M.; Zhao, Y.; Tian, Y.; Gou, G.; Tan, S.; et al. A wearable skinlike ultra-sensitive artificial graphene throat. *ACS Nano* **2019**, *13*, 8639–8647. [CrossRef]

39. Putra, T.E.; Abdullah, S.; Schramm, D.; Nuawi, M.Z.; Bruckmann, T. The need to generate realistic strain signals at an automotive coil spring for durability simulation leading to fatigue life assessment. *Mech. Syst. Sig. Process.* **2017**, *94*, 432–447. [CrossRef]

40. White, E.L.; Case, J.C.; Kramer, R.K. Multi-mode strain and curvature sensors for soft robotic applications. *Sens. Actuators A Phys.* **2017**, *253*, 188–197. [CrossRef]